Parametric analysis of a semi-closed-loop linear joule engine generator using argon and oxy-hydrogen combustion

Ngwaka, Ugochukwu; Wu, Dawei; Happian-Smith, Julian; Jia, Boru; Smallbone, Andrew; Diyoke, Chidiebere; Roskilly, Anthony Paul

DOI:
10.1016/j.energy.2020.119357

Document Version
Publisher's PDF, also known as Version of record

Citation for published version (Harvard):
Ngwaka, U, Wu, D, Happian-Smith, J, Jia, B, Smallbone, A, Diyoke, C & Roskilly, AP 2021, 'Parametric analysis of a semi-closed-loop linear joule engine generator using argon and oxy-hydrogen combustion', *Energy*, vol. 217, 119357. https://doi.org/10.1016/j.energy.2020.119357

Energy 217 (2021) 119357

Contents lists available at ScienceDirect

Energy

journal homepage: www.elsevier.com/locate/energy

Parametric analysis of a semi-closed-loop linear joule engine generator using argon and oxy-hydrogen combustion

Ugochukwu Ngwaka [a, e], Dawei Wu [b, *], Julian Happian-Smith [a], Boru Jia [c], Andrew Smallbone [d], Chidiebere Diyoke [e], Anthony Paul Roskilly [d]

[a] School of Engineering, Newcastle University, Newcastle Upon Tyne, NE1 7RU, United Kingdom
[b] Department of Mechanical Engineering, University of Birmingham, Birmingham, B15 2TT, United Kingdom
[c] School of Mechanical Engineering, Beijing Institute of Technology, Beijing, 100081, China
[d] Department of Engineering, Durham University, Durham, DH1 3LE, United Kingdom
[e] Faculty of Engineering, Enugu State University of Science and Technology, PMB 01660, Enugu, Nigeria

ARTICLE INFO

Article history:
Received 20 April 2020
Received in revised form
28 October 2020
Accepted 14 November 2020
Available online 19 November 2020

Keywords:
Linear joule engine generator
Argon-oxy-hydrogen combustion
Thermodynamic model
Zero carbon emissions

ABSTRACT

The paper introduces a novel semi-closed-loop Linear Joule Engine Generator (LJEG) using argon as the major working fluid and oxy-hydrogen combustion for heat addition. The linear compressor and expander in the LJEG apply double-acting piston configuration to maximise power density, and an oxy-hydrogen-argon reactor has ultra-high heat transfer efficiency and emits ultimate zero carbon, NOx, and particulate emissions. The proposed LJEG is developed from a previous lab-scale LJEG prototype using air as the working fluid. A comparison study demonstrates the advantages of the new conceptual design; substituting air with argon as the major working fluid resulted in increased system speed, decreased indicated power, and over 60% indicated efficiency improvement. A further parametric analysis was conducted using a validated model to reveal the influence of different intake and exhaust valve timing, compressor/expander diameter ratio, electric load, and operating temperature. The analysis shows that the system efficiency decreases with the extended intake duration, but it could be improved with the extension of expander exhaust duration. Power output increases with longer expander intake duration, however, its relationship with diameter ratio of compressor and expander is dependent on adopted expander exhaust valve timing, a peak power output of 4.7 kW could be achieved at expander intake temperature of 1073 K. System operating temperature for the optimal performance is also highly dependent on valve timings. Piston stroke length is adversely affected by an increase in compressor/expander diameter ratio and operating temperature. Peak system efficiencies of 40% and 60% could be achieved when the compressor/expander diameter ratio is 0.70 and 0.93, respectively.

1. Introduction

The Paris Agreement set a global target to keep a global temperature rise this century well below 2° Celsius above pre-industrial levels, which requires strong responses from the governments and industries to reduce carbon emissions. In 2019, the UK became the first major economy in the world to pass laws to bring all its greenhouse gas (GHG) emissions to net-zero by 2050, which demands rapid development and implementation of innovative decarbonisation technologies to achieve the target. Internal combustion engines (ICEs) consuming fossil fuels are still playing a pivotal role in transport, power generation and industries in the foreseeable future. With the increasing demands of electrification in transport and zero carbon emissions in industries, a new engine-generator technology, which can eliminate carbon emissions and minimise emissions of NOx and particular matters (PMs) is highly desired to compete with emerging fuel cells and batteries as an alternative power source in many applications. The concept of Linear Joule Engine Generator (LJEG) was first proposed by Mikalsen and Roskilly [1] for a potential application in micro-scale Combined Heat and Power (CHP) systems. The first design of LJEG was presented [2], and a first working prototype has been developed and has been in operation [3]. The LJEG is considered to combine the principles of the Reciprocating Joule Cycle Engines

* Corresponding author.
E-mail address: d.wu.1@bham.ac.uk (D. Wu).

https://doi.org/10.1016/j.energy.2020.119357

Abbreviations

ArH_2R	Argon−Hydrogen Reactor
BDC	Bottom Dead Centre
CER	Compressor/Expander diameter Ratio
CHP	Combined Heat and Power
ECU	Engine Control Unit
EEVC	Expander Exhaust Valve Closing
EEVO	Expander Exhaust Valve Opening
EIVC	Expander Intake Valve Closing
EIVO	Expander Intake Valve Opening
EVC	Exhaust Valve Closing
EVO	Exhaust Valve Opening
GLC	Generator load coefficient
IVC	Intake Valve Closing
ICE	Internal Combustion Engine
IVO	Intake Valve Opening
LEG	Linear Electric Generators
LJEG	Linear Joule Engine Generator
NOx	Oxides of Nitrogen
RJCE	Reciprocating Joule Cycle Engines
SP	Specific Power
TDC	Top Dead Centre

Nomenclature

A	Condenser total heat transfer area (m^2)
A_c	Compressor piston area (m^2)
A_d	Reference flow area (m^2)
A_e	Expander piston area (m^2)
A_{re}	Reactor surface area (m^2)
C_d	Discharge coefficient (−)
$\overrightarrow{F_e}$	Pressure force from linear expander (N)
$\overrightarrow{F_{el}}$	Pressure force from left chamber of the expander (N)
$\overrightarrow{F_{er}}$	Pressure force from right chamber of the expander (N)
$\overrightarrow{F_c}$	Pressure force from linear compressor (N)
$\overrightarrow{F_{cl}}$	Pressure force from left chamber of the compressor (N)
$\overrightarrow{F_{cr}}$	Pressure force from right chamber of the compressor (N)
F_f	Friction force (N)
F_{fd}	Dry contact friction force (N)
F_{fp}	Pressure friction force (N)
$\overrightarrow{F_g}$	Generator force (N)
G	Linear generator load constant ($N/(m \cdot s^{-1})$)
h	Coefficient of heat transfer in the expander ($W/m^2 \cdot K$)
h_a	Enthalpy of argon flowing into the condenser (J/kg)
h_{ac}	Enthalpy of argon flowing out of the condenser (J/kg)
h_{cw}	Enthalpy of water flowing out of the condenser (J/kg)
h_e	Specific enthalpy of the mass flow through the expander (J/kg)
h_{in}	Specific enthalpy of the intake gas to the reactor (J/kg)
h_s	Enthalpy of saturated steam flowing into the condenser (J/kg)
h_{out}	Specific enthalpy of the exhaust gas from the reactor (J/kg)
L	Length (m)
m	Moving mass (kg)
$\dot{m}$	Mass flowrate through valves (kg/s)
$\dot{m}_a$	Argon content flowing into the condenser (kg/s)
$\dot{m}_c$	Mass flowrate through the compressor (kg/s)
$\dot{m}_{cf}$	Condenser cooling fluid flow rate (kg/s)
$\dot{m}_f$	Mass flowrate of the hydrogen injected to the reactor (kg/s)
$\dot{m}_e$	Mass flowrate through the expander (kg/s)
$\dot{m}_{in}$	Mass flow into the reactor (kg/s)
$\dot{m}_s$	Steam flowing into the condenser (kg/s)
$\dot{m}_{out}$	Mass flowrate out of the reactor (kg/s)
p_c	Pressure in the compressor (Pa)
p_{cl}	Pressure in the left compressor (Pa)
p_{cr}	Pressure in the right compressor (Pa)
p_d	Downstream pressure (Pa)
p_e	Pressure in the expander (Pa)
p_{el}	Pressure in the left expander (Pa)
p_{er}	Pressure in the right expander (Pa)
p_u	Upstream pressure (Pa)
$p_{i/o}$	Suction or discharge compressor fluid pressure (Pa)
P	Generator power output (W)
Pd	Product
$\dot{Q}$	Heat duty (J/s)
$\dot{Q}_{add}$	Heat addition (J/s)
$\dot{Q}_{cf}$	Condenser cooling fluid heat absorption quantity (J/s)
$\dot{Q}_h$	Heat flow rate (J/s)
$\dot{Q}_{ht}$	Heat transfer from the reactor to the environment (J/s)
Q_{hyd}	Energy carried in hydrogen (W)
$\dot{Q}_{rx}$	Heat of reaction (J/s)
Re	Reagent
T_0	Temperature of the environment (K)
T_{cfo}	Condenser outlet temperature of the cooling fluid (K)
T_{cfi}	Condenser inlet temperature of the cooling fluid (K)
T_c	Average outlet temperature of the fluid flowing out of the condenser (K)
T_{in}	Temperature of the intake mass flow into the reactor (K)
T_{out}	Temperature of the exhaust mass flow out of the reactor (K)
T_{re}	Temperature in the reactor (K)
T_u	Temperature of upstream (K)
T_w	Average surface temperature of expander cylinder wall (K)
x	Piston displacement (m)
$\dot{x}$	Piston sliding velocity (m/s)
$\dot{x}_m$	Mean piston velocity (m/s)
$\ddot{x}$	Piston acceleration (m/s^2)
$\ddot{x}_m$	Mean piston acceleration (m/s^2)
U	Overall heat transfer coefficient ($W/K \cdot m^2$)
V	Instantaneous cylinder volume (m^3)
V_c	Working volume of linear compressor (m^3)
V_e	Working volume of linear expander (m^3)
α	Coefficient of the reactor heat transfer ($W/K \cdot m^2$)
γ	Heat capacity ratio (−)
ΔT_{lm}	The logarithmic mean temperature difference (K)
η	System efficiency (%)
$\rho_{i/o}$	Suction/discharge compressor fluid density (kg/m^3)

(RJCE) and Linear Electric Generators (LEG), which can easily adapt to almost any fuels without significant engine modifications because the energy input is external, compared to conventional ICEs. This makes it a potential candidate of zero-carbon power source in the future hydrogen economy.

There has been growing research interests in RJCE and LEG technologies. Researchers at Plymouth University [4] presented a thermodynamic model of RJCE, with a traditional crankshaft mechanism. The simulation results predicted a thermal efficiency of over 50%. Creyx et al. developed a static numerical model of an open-loop RJCE [5]. The reported thermal efficiency was 37% at a pressure ratio of 6 and a low operating temperature of 650 °C after optimisation. Moss, Roskilly, and Nanda [6] presented a similar study on an RJCE for CHP application and reported a thermal efficiency of 38%. The results indicated that the system's thermal efficiency is proportional to the operating pressure ratio and peak temperature. A study on open-loop Joule Cycle Engine for micro co-generation systems [7], suggested that the use of a regeneration cycle for waste heat recovery can enhance engine performances, and thermal efficiency of 23% was predicted at a pressure ratio of 4. Results from a similar study indicated that with a temperature of 900 K, an indicated efficiency of over 42% could be achieved at a pressure ratio between 2 and 3.2 [8]. Wu, Jalal, and Baker [9] presented an integrated model and design of LJEG. The simulation results predicted an electric conversion efficiency of 30% at the maximum temperature of 790 °C and the pressure ratio of 6.5. The research team from Newcastle University also presented and validated a detailed model of an open-loop LJEG [10]. The model predicted an electric conversion efficiency of 30% at a pressure ratio of 7 and a maximum temperature of 800 °C. Ndame and Stouffs presented a design and a thermodynamic model of open cycle air-standard liquid piston RJC engine, suitable for low power solar energy conversion, micro-CHP applications and waste heat recovery [11]. The results indicated that thermal efficiency of over 35% could be achieved with an expander inlet temperature of 633 K, pressure ratio of 3 and engine speed of 37.8 rpm. Results also revealed that similar RJC engine configuration indicated efficiency decreased with increased engine rotation speed [12].

However, most of the existing research on RJCE and LJEG focused on development of engine generator and performance prediction based on open-loop technology, and very few works have investigated use of zero carbon fuels. An ongoing project conducted by the research team is trying to address this gap, which proposes a semi-closed-loop LJEG using hydrogen fuel and continuous external combustion for heat addition. To eliminate both NOx and carbon emissions when hydrogen combustion is applied, an alternative working fluid instead of air and oxy-hydrogen combustion are investigated for the proposed LJEG in this paper.

Hydrogen combustion has been extensively tried in both traditional ICEs and non-traditional combustion engines [13] but using air as an oxidiser and working fluid results in inevitable NOx emissions. Replacing nitrogen with noble gas in oxy-hydrogen combustion can eliminate the production of NOx caused by the absence of nitrogen and leads to increased combustion flame temperatures [14,15]. It also has the advantage of significantly boosting the cycle efficiency due to the higher specific heat ratio of noble gases [16]. There seems to be an agreement on the choice of argon to other noble gases in hydrogen-oxygen-noble gas combustion technology. Shahsavan, Morovatiyan and Mack [15] analysed the use of hydrogen fuel in constant volume combustion and compared the mixtures of oxygen with nitrogen, argon, or xenon. The results indicated that argon appears to be a better-working fluid for hydrogen combustion. However, both argon and xenon provide higher temperatures and OH mass fractions in comparison to nitrogen; argon also shows a far better mixing rate of the injected fuel compared to xenon due to higher diffusivity [15]. Fuel diffusivity is known to be a vital parameter desired, and high diffusivity enhances better fuel and oxidiser mixing in non-premixed combustion [17]. Argon is abundantly available; it is relatively inexpensive compared with other available noble gases and is easily and readily obtainable as a by-product of cryogenic air separation [18]. Additionally, argon gas facilitates the creation of gas-tight seals [19], and the specific heat ratio of argon does not decrease at high temperatures compared to nitrogen [20]. Most of the reported studies on argon-oxy-hydrogen combustion are on ICEs. A research team from Tongji University experimentally explored argon-oxy-hydrogen combustion in spark-ignition engine [21], the results indicated that higher Indicated mean effective pressure (IMEP) and better combustion stability is achieved with argon-oxy-hydrogen combustion compared with hydrogen-air combustion [22], and the argon-oxy-hydrogen mixture could promote combustion reaction [23]. Similarly, researchers from University of California [24–26] Kyoto University and Universiti Kebangsaan [20,27,28] experimentally investigated argon-oxy-hydrogen combustion in an open-loop ICE and reported an efficiency improvement. Researchers from Toyota Motor Corporation [19] investigated semi-closed-loop argon-oxy-hydrogen combustion on ICE. Test results indicated an efficiency improvement of 28% at a pressure ratio of 6.

Compared to ICEs using argon-oxy-hydrogen combustion concept, LJEG has its inherent advantage to make the combustion concept integrated into the engine. In this study, a "first-of-its-kind" semi-closed-loop LJEG powered by argon-oxy-hydrogen combustion is proposed, modelled and optimised. The effects of the geometric and operational parameters on the operability and performance of an LJEG were examined. The proposed LJEG consists of five main components, i.e., a positive displacement compressor, a positive displacement expander, a linear electric generator, a condenser, and an isobaric external combustion chamber. The research team developed an experimentally validated model with Matlab/Simulink. Advantages and limitations of different geometric and operational parameters on the performance indicators of an LJEG were evaluated, aiming to guide LJEG design under various operational variables. The reactor model validation is performed with the data from Drell and Belles [29], and the dynamic and thermodynamic model is validated with the test data from an LJEG prototype developed by the research team.

2. System description and model architecture

2.1. System information

The schematic configuration of the LJEG prototype developed in the laboratory is shown in Fig. 1a. Two double-acting pistons, rigidly connected with a rod, are oppositely placed in the expander (on the left side) and the compressor (on the right side) respectively, as shown in Fig. 1a. Intake and exhaust valves are located on both ends of the expander and the compressor to draw in and expel a working fluid. The thermodynamic cycle commenced from the compressor, where the working fluid was compressed before the compressed working fluid is fed into the external combustor. Hydrogen is supplied to and burns in the argon-hydrogen reactor (ARH_2-R), where the energy of the working fluid is increased at a constant pressure. The working fluid with elevated temperature and energy level from the combustor is injected into the expander to produce expansion work, which is utilised to drive the compressor for pressure build-up and the linear generator for electricity. The theoretical thermodynamic cycle of a semi-closed cycle LJEG is shown in Fig. 1b, and this consisted of four

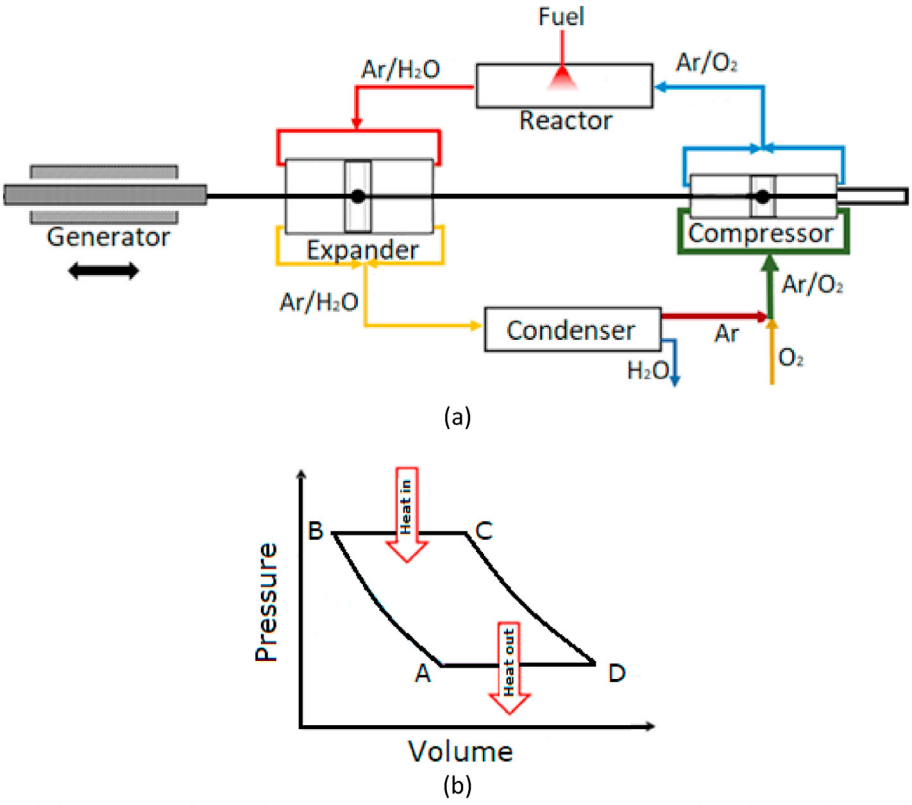

Fig. 1. (a) Linear Joule Cycle Engine Generator configuration. (b) Joule Cycle P–V diagram.

processes. A-B is the adiabatic and reversible compression of argon/oxygen mixture in the compressor. B–C is the constant pressure fuel combustion - idealised as constant pressure heat addition. C-D is the reversible and adiabatic expansion when hot, and high-pressure gases enter two separate expander chambers and expand in the chambers alternatively. This expansion pushes the piston resulting in linear back and forth motion. The mechanical power from the linear motion partly drove the compressor piston for the compression process, and the remaining power was the output to drive the linear generator for electricity generation. D-A is the constant pressure heat rejection process. This involves the constant pressure ejection of heat to the environment through the condenser. Alongside this, water is removed from the cycle, leaving only pure argon for the next cycle. The detailed engine configuration and the validated numerical model were presented in the paper [3]. An updated model reflecting the configuration with new components, e.g. an oxy-hydrogen-argon combustor, a condenser, etc. is described in the following section.

Table 1
Base case input parameters.

	Parameters [Unit]	Value
	Moving mass [kg]	8.0
Linear expander	Maximum stroke [mm]	118
	Effective bore [mm]	85
	Inlet pressure [bar]	7.0
	Inlet temperature [K]	1070
	IVO [mm]	TDC
	IVC [mm]	20
	EVO [mm]	BDC
	EVC [mm]	TDC
Linear compressor	Effective bore [mm]	70
	Inlet pressure [bar]	1.0
	Outlet pressure [bar]	7.0
	IVO [mm]	BDC
	IVC [mm]	TDC
Reactor	Inlet pressure [bar]	7.0
	Inlet temperature [K]	420

2.2. Model architecture

The piston assembly and the linear generator translator in the middle of the pistons are the only moving part in LJEG, and the forces acting on the piston assembly/translator determines its dynamics. The forces acting on the piston assembly include the gas pressure forces from the linear compressor and the expander, the frictional forces, the resistant force from the linear generator and the inertia of the moving mass. These forces represented according to Newton's Second Law as:

$$\vec{F_e} + \vec{F_c} + \vec{F_g} + \vec{F_f} = m\ddot{x} \quad (1)$$

$$\vec{F_e} = \overrightarrow{F_{el}} + \overrightarrow{F_{er}} \quad (2)$$

$$\vec{F_c} = \overrightarrow{F_{cl}} + \overrightarrow{F_{cr}} \quad (3)$$

where $\vec{F_e}$ (N) represents the resultant gas pressure force from the linear expander; $\overrightarrow{F_{er}}$ (N) represents the pressure force from the right chamber of the linear expander; $\overrightarrow{F_{el}}$ (N) represents the gas pressure force from the left chamber of the linear expander. $\vec{F_c}$ (N) represents the resultant gas pressure force from the linear compressor; $\overrightarrow{F_{cr}}$ (N) represents the gas pressure force from the

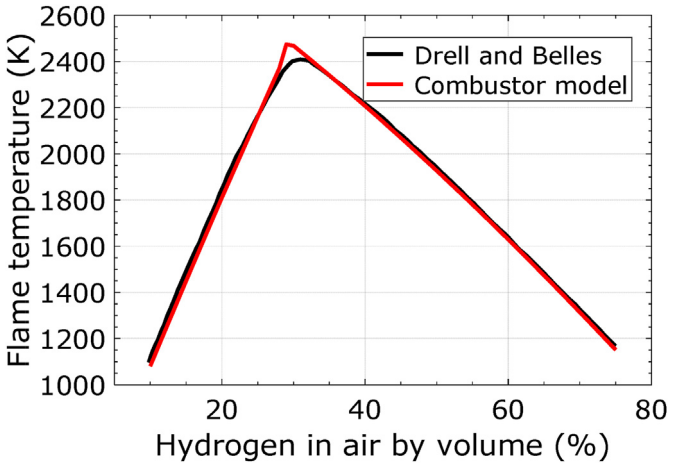

Fig. 2. Flame temperatures for hydrogen-air mixtures.

right chamber of the compressor; $\overrightarrow{F_{cl}}$ (N) represents the gas pressure force from the left chamber of the linear compressor. $\overrightarrow{F_f}$ (N) denotes the friction force, $\overrightarrow{F_g}$ (N) denotes the generator force, $\ddot{x}$ (m/s^2) represents piston acceleration, m (kg) is the moving mass. The gas pressure forces from both chambers of the linear compressor and expander were obtained using the in-cylinder pressure and cross-section area of the piston.

$$\overrightarrow{F_{el}} = p_{el} \cdot A_e \tag{4}$$

$$\overrightarrow{F_{er}} = p_{er} \cdot A_e \tag{5}$$

$$\overrightarrow{F_{cl}} = p_{cl} \cdot A_c \tag{6}$$

$$\overrightarrow{F_{cr}} = p_{cr} \cdot A_c \tag{7}$$

where p_{er} (Pa) and p_{el} (Pa) represent the in-cylinder pressure in the right and the left chamber of the expander, respectively. p_{cr} (Pa) and p_{cl} (Pa) represent the in-cylinder pressure in the right and the left chamber of the compressor, respectively. A_c (m^2) and A_e (m^2) represent the piston cross-section area of the compressor and the expander, respectively.

2.2.1. Dynamic and thermodynamic model

By applying ideal gas equations and the conservation of energy principle in a control volume on the in-cylinder charge, yields Equation (8) for pressure calculation in the expander [3] and Equation (9) for pressure calculation in the compressor [30].

Table 2
Prototype specifications and simulation input parameters [30].

	Parameters [Unit]	Value
Expander	Maximum stroke [mm]	120.0
	Effective bore [mm]	80.0
	Inlet pressure [bar]	2.7
	Inlet temperature [K]	473.0
	Valve diameter [mm]	32.5
	Valve lift [mm]	8.13
Compressor	Maximum stroke [mm]	120.0
	Effective bore [mm]	70.0
	Inlet pressure [bar]	1.0
	Outlet pressure [bar]	2.7

Table 3
Prototype test results and simulation results.

	Experiment	Simulation	Simulation
Working fluid	Air	Air	Argon
Cycle	open	open	Closed
Frequency (Hz)	5.26	5.27	5.59
Flowrate (kg/s)	9.45×10^{-3}	9.73×10^{-3}	11.31×10^{-3}
Indicated power (W)	762	765	734
Indicated efficiency (%)	40	39	62.5

$$\frac{dp_e}{dt} = \frac{\gamma - 1}{V_e}\left(-\frac{dQ_h}{dt}\right) - \frac{p\gamma}{V_e}\frac{dV_e}{dt} + \frac{\gamma - 1}{V_e}\sum_i \dot{m}_e h_e \tag{8}$$

$$\frac{dp_c}{dt} = \gamma\left(\frac{p_{i/o}}{V_c\,\rho_{i/o}}\dot{m}_c - \frac{\dot{x}p_c}{x}\right) \tag{9}$$

where γ represents the working fluid specific heat capacity ratio; $\dot{m}_e$ (kg/s) represents the mass flowrate through the expander; Q_h (J) denotes the heat flow across the cylinder wall; p_e (Pa) and V_e (m^3) represent the pressure inside the expander and expander working volume respectively; h_e (J/kg) denotes the specific enthalpy of the mass flow through the expander. p_c (Pa) represents the pressure inside the compressor; $p_{i/o}$ (Pa) denotes the suction/discharge pressure from the compressor; $\rho_{i/o}$ (kg/m^3) denotes the compressor suction/discharge density; $\dot{m}_c$ (kg/s) represents the compressor suction/discharge mass flowrate. V_c (m^3) denotes the compressor working volume; x (m) denotes the piston displacement; $\dot{x}$ (m/s) represents the piston sliding velocity. Further information on a detailed thermodynamic process modelling of the expander and the compressor of an LJEG, could be accessed in Ref. [10].

The linear electric machine generates an electrical current through the continuous back and forth movement of the piston assembly rod, the piston assembly rod was placed inside the stator. The load force of the linear electric generator is assumed to be proportional to the current generated according to electromagnetic theory, and its direction is continuously opposite to the piston velocity [31], the resistance force from the generator is described as:

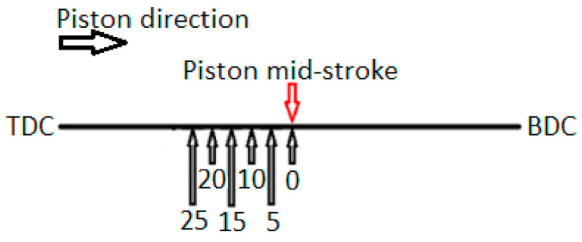

a. Illustration of the left expander intake valve timing.

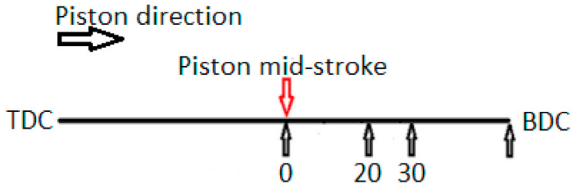

b. Illustration of the right expander exhaust valve timing.

Fig. 3. a. Illustration of the left expander intake valve timing. b. Illustration of the right expander exhaust valve timing.

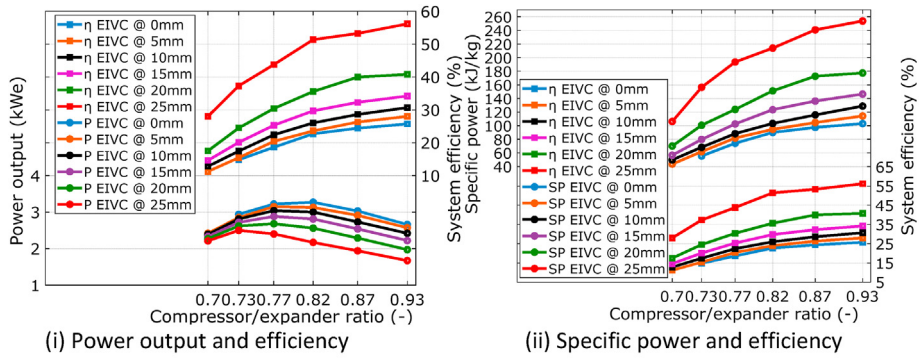

a. Power output, specific power and system efficiency when the EEVC at 20mm after the mid-stroke.

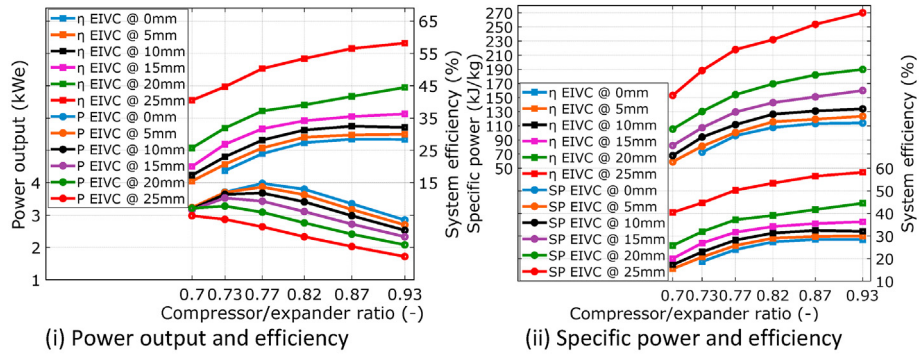

b. Power output, specific power and system efficiency when the EEVC at 30mm after the mid-stroke.

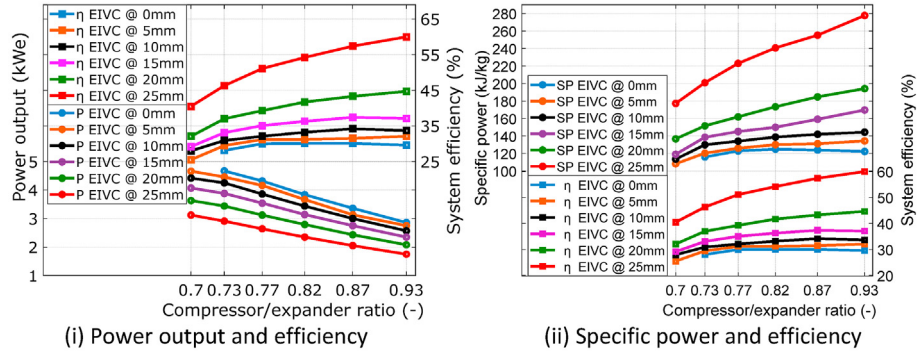

c. Power output, specific power and system efficiency when the EEVC at BDC.

Fig. 4. a. Power output, specific power and system efficiency when the EEVC at 20 mm after the mid-stroke. b. Power output, specific power and system efficiency when the EEVC at 30 mm after the mid-stroke. c. Power output, specific power and system efficiency when the EEVC at BDC.

$$\overrightarrow{F_g} = -G\dot{x} \tag{10}$$

where G (N/(ms^{-1})) represents the generator load constant; which is ascertained from the physical parameters of the generator design specifications and the external load of the circuit [32] and $\dot{x}$ (m/s) represents the piston velocity.

The frictional force model in LJEG was studied in the previous paper [30] which was presented as follows. The total friction force F_f was estimated as a combination of dry contact friction and friction due to pressure loading, as described in the equations below:

$$F_f = F_{fd} + F_{fp} \tag{11}$$

where F_f (N) denotes the total friction force; F_{fd} (N) represents the contact friction; F_{fp} represents the friction force due to pressure loading.

2.2.2. Combustor and fluid control model

The combustor model comprising a reactor, mixers, and pure and mixed substance flow sources using Thermolib: a toolbox of thermodynamic property library, which calculates the thermodynamic properties of fluids based on its composition in MATLAB/Simulink environment. The chemical composition of the fuel/oxidiser mixture was defined using the Thermolib library. However,

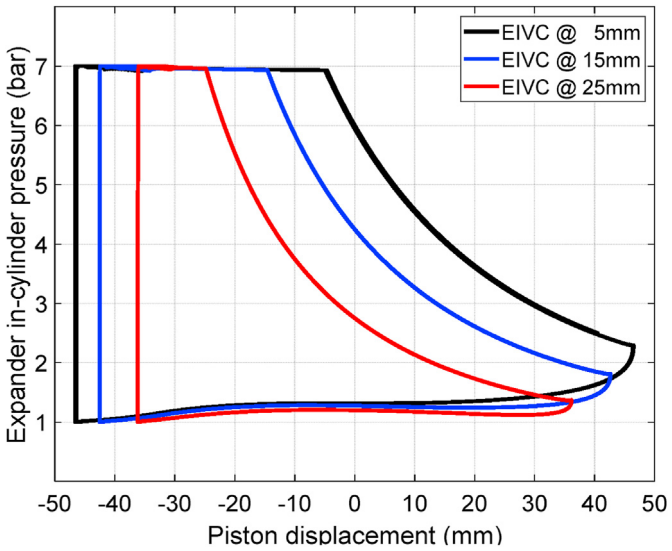

Fig. 5. Expander in-cylinder pressure with EIVC at 5 mm, 15 mm and 25 mm, EEVC at BDC, and CER of 0.823.

argon is not currently among the species in the Thermolib library database; therefore the thermo-physical properties of argon and the NASA coefficients for calculating thermodynamic and transport properties of argon were added to the library database. The reactor sub-model computes the outgoing flow after one/each reaction by employing the first law of thermodynamics for a chemical reaction. The sub-model also considers the heat exchange with the surrounding environment. The engine control unit (ECU) calculates the quantity of oxygen supplied to the compressor based on the temperature and mass of argon available in the compressor and the target operating temperature in the expander. The quantities of oxygen and hydrogen supplied per stroke are the right amount that would react to raise the temperature of argon to the targeted expander intake temperature. Similarly, the ECU calculates the quantity of hydrogen injected into the combustor based on the mass of oxygen available in the oxygen-argon mixture from the compressor. Therefore, the content of the working fluid going into the expander would be argon gas and steam.

The general combustion equation for hydrogen and oxygen becomes:

$$2H_2 + O_2 \rightarrow 2H_2O \tag{12}$$

The first law of thermodynamics for a chemical reaction is expressed as:

$$\sum_{Re} \dot{m}_{in} h_{in} = \sum_{Pd} \dot{m}_{out} h_{out} + \dot{Q}_{add} \tag{13}$$

$$\dot{Q}_{add} = \dot{Q}_{rx} - \dot{Q}_{ht} \tag{14}$$

$$h_{in} = c_{pin} \cdot T_{in} \tag{15a}$$

$$h_{out} = c_{pout} \cdot T_{out} \tag{15b}$$

$$\dot{Q}_{ht} = \alpha A_{re} (T_{re} - T_0) \tag{16}$$

where $\dot{m}_{in}$ (kg/s) is the mass flow into the reactor; h_{in} (J/kg) is the specific enthalpy of the intake gas to the reactor; $\dot{m}_{out}$ (kg/s) is the mass flow rate out of the reactor; h_{out} (J/kg) is the specific enthalpy of the exhaust gas from the reactor; c_{pin} (J/kg·K) is the specific heat capacity at constant pressure for the intake fluid; c_{pout} (J/kg·K) is the specific heat capacity at constant pressure for the exhaust gas from the reactor. T_{in} (K) is the temperature of the intake mass flow into the reactor; T_{out} (K) is the temperature of the exhaust mass flow out of the reactor. $\dot{Q}_{add}$ (J/s) is the heat addition; $\dot{Q}_{rx}$ (J/s) is the heat of reaction; $\dot{Q}_{ht}$ (J/s) is the heat transfer from the reactor to the environment; $\dot{m}_f$ (kg/s) is the mass flow rate of the hydrogen injected to the reactor. α (W/K·m^2) is the coefficient of the heat transfer model; A_{re} (m^2) is the surface area of the reactor; T_{re} (K) is the temperature in the reactor and T_0 (K) is the temperature of the environment.

2.2.3. Condenser

The main factor considered in the mathematical model of the condenser is heat transfer performance. The heat transfer rate for steam/water and argon flowing through a condenser is given by

$$\dot{Q} = \dot{m}_s(h_s - h_{cw}) + \dot{m}_a(h_a - h_{ac}) \tag{17}$$

where $\dot{Q}$ (J/s) is the condenser heat duty, $\dot{m}_s$ (kg/s) is the content of steam flowing into the condenser. h_s (J/kg) is the enthalpy of saturated steam flowing into the condenser, h_{cw}(J/kg) is the enthalpy of water flowing out of the condenser, $\dot{m}_a$ (kg/s) is the argon content flowing into the condenser, h_a (J/kg) is the enthalpy of argon flowing into the condenser, h_{ac} (J/kg) is the enthalpy of argon flowing out of the condenser. However, the heat transfer rate is approximated by:

$$\dot{Q} = UA\Delta T_{lm} \tag{18}$$

where U (W /(m^{2}K)) is the overall heat transfer coefficient, A (m^2) is the total heat transfer area and ΔT_{lm} (K) is the logarithmic mean temperature difference.

$$\Delta T_{lm} = \frac{T_{cfo} - T_{cfi}}{ln\left(\frac{T_c - T_{cfi}}{T_c - T_{cfo}}\right)} \tag{19}$$

where T_{cfo} (K) is the outlet temperature of the cooling fluid, T_{cfi} (K) is the inlet temperature of the cooling fluid and T_c(K) is the average outlet temperature of the fluid flowing out of the condenser.

The energy balance of the cooling fluid yields

$$\dot{Q} - \dot{Q}_{cf} = UA\Delta T_{lm} - \dot{m}_{cf} C_p \left(T_{cfo} - T_{cfi}\right) = 0 \tag{20}$$

where C_p (J/(kg K)) is the cooling fluid heat capacity, $\dot{Q}$ (J/s) is the condenser heat duty, $\dot{Q}_{cf}$ (J/s) is the cooling fluid heat absorption quantity and $\dot{m}_{cf}$ (kg/s) is the cooling fluid flow rate.

The system efficiency calculation is as shown in Equation (21) and it with the assumption that hydrogen is the only energy carrier gas among all other gases in the system.

$$\eta = \frac{P}{Q_{hyd}} \times 100\% \tag{21}$$

where η (%) is the system efficiency, P (W) is the generator power output and Q_{hyd} (W) is the input energy provided by hydrogen.

2.3. Input parameters

The input parameters are listed in Table 1. The inlet pressure of the reactor is set to be the same as the outlet pressure of the

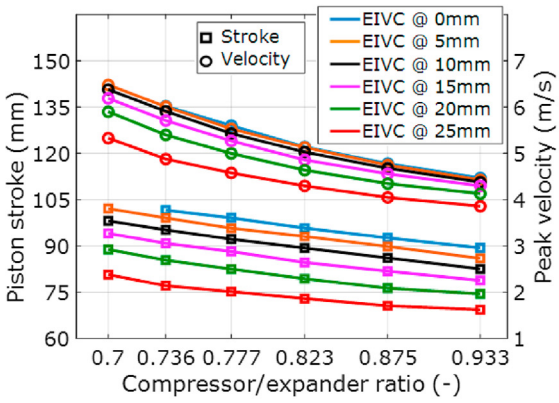

a. Piston stroke and peak velocity when the EEVC at 20mm after mid-stroke.

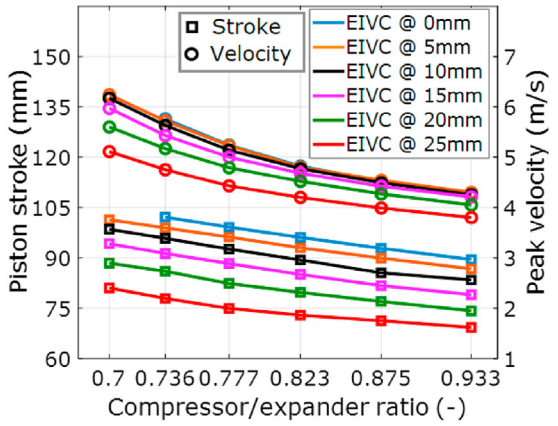

b. Piston stroke and peak velocity when the EEVC at 30mm after mid-stroke.

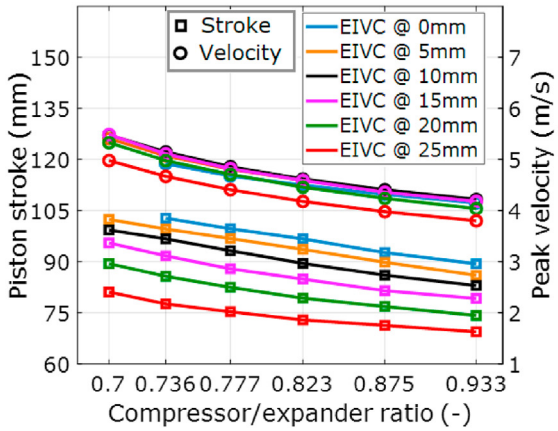

c. Piston stroke and peak velocity when the EEVC at BDC.

Fig. 6. a. Piston stroke and peak velocity when the EEVC at 20 mm after mid-stroke. 6 b. Piston stroke and peak velocity when the EEVC at 30 mm after mid-stroke.6c. Piston stroke and peak velocity when the EEVC at BDC.

compressor. The mass flowrate from the compressor to the reactor is fluctuating in terms of the system dynamics and thermodynamic equilibrium.

The valves were actuated based on the piston displacement; therefore, the fluid inlet and outlet durations of both the compressor and expander are significantly affected by the piston speed and the piston lifting and descending profiles.

2.4. Simulation model development

The simulation model was developed in Matlab/Simulink coupled with Matlab/Thermolib.

While Matlab/Thermolib was used to develop the sub-models of combustion, condenser, and fluid flow, the rest of the sub-models were developed in Matlab/Simulink. The sub-models were activated in terms of the piston displacement and velocity using the State Flow Chart function in Simulink. The model closed-loop status was achieved by the use of both initial-conditions blocks and a

buffer. All the participating species were selected from Thermolib library database and added to Thermolib Model Setup. All the added species were allowed in both liquid and gas phase, and the balancing time from start to stop is 60 s and 100 s respectively. Fixed step automatic solver was utilised, with a fixed step size of 1 × 10e-6s. The design parameters for the simulation and initial-boundary parameters were set before simulation. The piston displacement, piston velocity, and combustor fluid outlet temperature were selected as the target outputs to determine the valve timings. The valve timings for opening and closing were adjusted to optimise the scavenging process. The expander intake valve opening (EIVO) event and the expander exhaust valve opening (EEVO) event were triggered when the piston reaches its TDC and BDC, respectively. The expansion process of the expander was initiated after the EIVO event was triggered.

3. Results and discussions

The dynamic and thermodynamic model of an LJEG without integrating the combustion model was investigated, and the results have been validated with the test data from a lab-scale prototype in the previous papers [3,30]. In this section, the emphasis is on the hydrogen combustion model validation and preliminary justification on the use of argon as the working fluid rather than air and optimisation of operational and geometric parameters of an LJEG.

3.1. Combustion model validation

Flame temperature is one of the unique and vital factors that characterise the combustion behaviour of a specific mixture of fuel and oxidant. A comparison between the simulated data from the hydrogen-air combustion model and the measured data from Drell and Belles [29] was carried out and represented in Fig. 2.

The results in Fig. 2 are for constant pressure combustion, with a pressure of 1.01325 bar and an initial mixture temperature of 298 K. The simulated temperature data generally corresponds to the measured data within the range of operating temperature expected on an LJEG, which is entirely below 2350 K. Some discrepancy existed between the measured and the simulated data for temperature above 2350 K. The regional discrepancy existed because the conversion rate of hydrogen was fixed in the combustion model and did not vary with temperature. However, since the model could robustly predict the flame temperature for oxy-hydrogen combustion in a nitrogen atmosphere, it would be right to conclude that the model could reasonably predict the flame temperature for oxy-hydrogen combustion in an argon atmosphere.

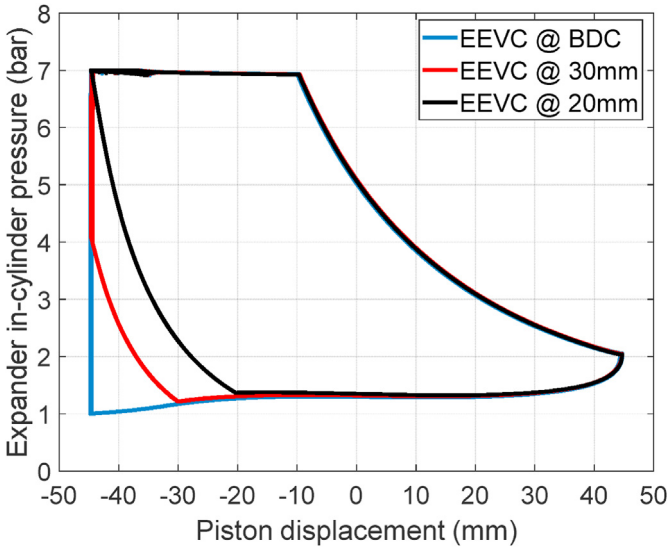

Fig. 7. Expander in-cylinder pressure with EIVC at 10 mm, EEVC at BDC, 30 mm and 20 mm, CER 0.823.

3.2. Alternative working fluid justification

The simulation results for a semi-closed-loop argon-oxy-hydrogen LJEG and an open loop air-standard LJEG model were compared to the test data from an open loop air-standard LJEG prototype developed at Newcastle University which was presented in Ref. [30]. The open and semi-closed-loop models parametric specifications were set to be identical with the prototype, and the simulation and prototype input parameters are listed in Table 2.

The results of the simulation are presented in Table 3. The results of open cycle air-standard operation show a good alignment with the test data. While argon was employed as the working fluid and all other parameters were kept the same, the results indicated an increased system speed, a decrease in indicated power, and over 60% improvement in indicated efficiency. The major efficiency improvement is attributed to the thermo-physical properties of argon; the specific heat ratio of argon gas is higher compared to air, and the specific heat ratio of argon does not decrease at high temperatures compared to air [20]. Additionally, the constant pressure specific heat capacity of air increases with temperature, but the constant pressure specific heat capacity of argon remains constant at higher temperatures [33]. It implies that more energy would be needed in the combustor per Kelvin temperature rise with air being used as the working fluid, but such increased energy demand will not occur if argon was used. The target design pressure ratio for the LJEG operation is about 7, and it is expected that with argon as the working fluid, the system would replicate a similar improved efficiency at such pressure ratio.

Apart from the thermo-physical property benefit of argon compared to air, zero emissions from oxy-hydrogen combustion with argon presence instead of air would be another major advantage. A recent study on hydrogen-powered air-standard free-piston engine generator indicated that oxides of nitrogen (NOx) emissions could be above 80 parts per million (ppm) [13]. However, NOx emissions would be eliminated in the proposed argon-oxy-hydrogen combustion of a semi-closed-loop argon-oxy-hydrogen LJEG.

3.3. Optimisation of operational and geometric variables

The simulation results for a semi-closed-loop argon-oxy-hydrogen LJEG at design conditions are presented in this section. The simulation input parameters can be seen in Table 1. Variations in compressor/expander diameter ratios, temperatures, and generator loads, and expander inlet and exhaust durations are considered in the simulation to reveal the relationships with performance indicators, e.g. power output, efficiency, specific power etc., which leads to optimisation of the proposed LJEG.

Influence of the ratio of the compressor and the expander diameters was investigated for different expander intake and exhaust valve timings. The valves were assumed to be completely open/close according to open/close command in the simulation model, and the valve response time was the same for valve open/close command in this study. The piston displacement and velocity feedback to the control loop for valve timing adjustment. The illustration of intake valve timing of the left expander is shown in Fig. 3a, the intake valve open command of the left expander was triggered when the piston reached its top dead centre (TDC) and the piston velocity was zero. The intake valve closed before or exactly at the mid-stroke. Six different intake valve timings were

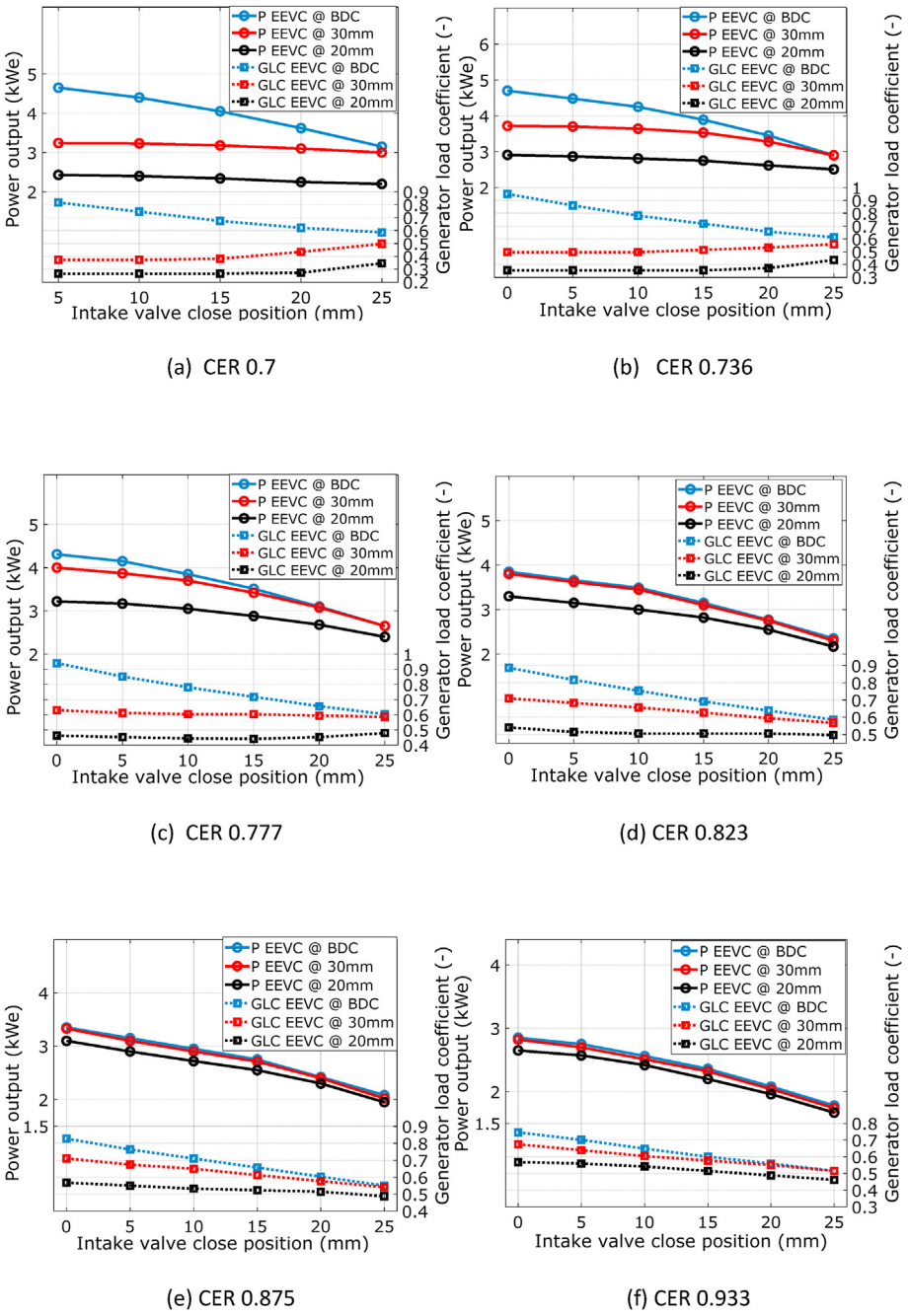

Fig. 8. Power output and GLC at different engine conditions.

investigated including Expander Intake Valve Closing (EIVC) at 25 mm, 20 mm, 15 mm, 10 mm, 5 mm before the mid-stroke and at the mid-stroke (0 mm before). The exhaust valve timing for the right expander is illustrated in Fig. 3b. The exhaust valve open command for the right expander was initiated when the piston reached its bottom dead centre (BDC), which was TDC for the left expander. Confusion of the interchanging nature of BDC and TDC of the left and right expander when in operation was eliminated by adopting the TDC and BDC of the left expander as the convention for this study. Three different expander exhaust valve timings were analysed and investigated, which were Expander Exhaust Valve Closing (EEVC) at 20 mm and 30 mm away from the mid-stroke and at exact BDC.

The compressor/expander ratio (CER) is the ratio of the diameter of the compressor to the diameter of the expander. The power output, specific power (power output divided by working fluid mass flowrate) and system efficiency versus compressor/expander ratio (CER) are shown in Fig. 4, which were generated with the model using the input parameters stated in Table 1. Fig. 4a(ii), 4 b(ii) and 4c(ii) show specific power and system efficiency at different engine conditions. It is clear that the specific power increased with system efficiency proportionally and have a similar trend with efficiency in all cases; therefore, more attention is given to system efficiency and power output rather than specific power consequently in the paper.

Fig. 4 display the operational CER range and the possible

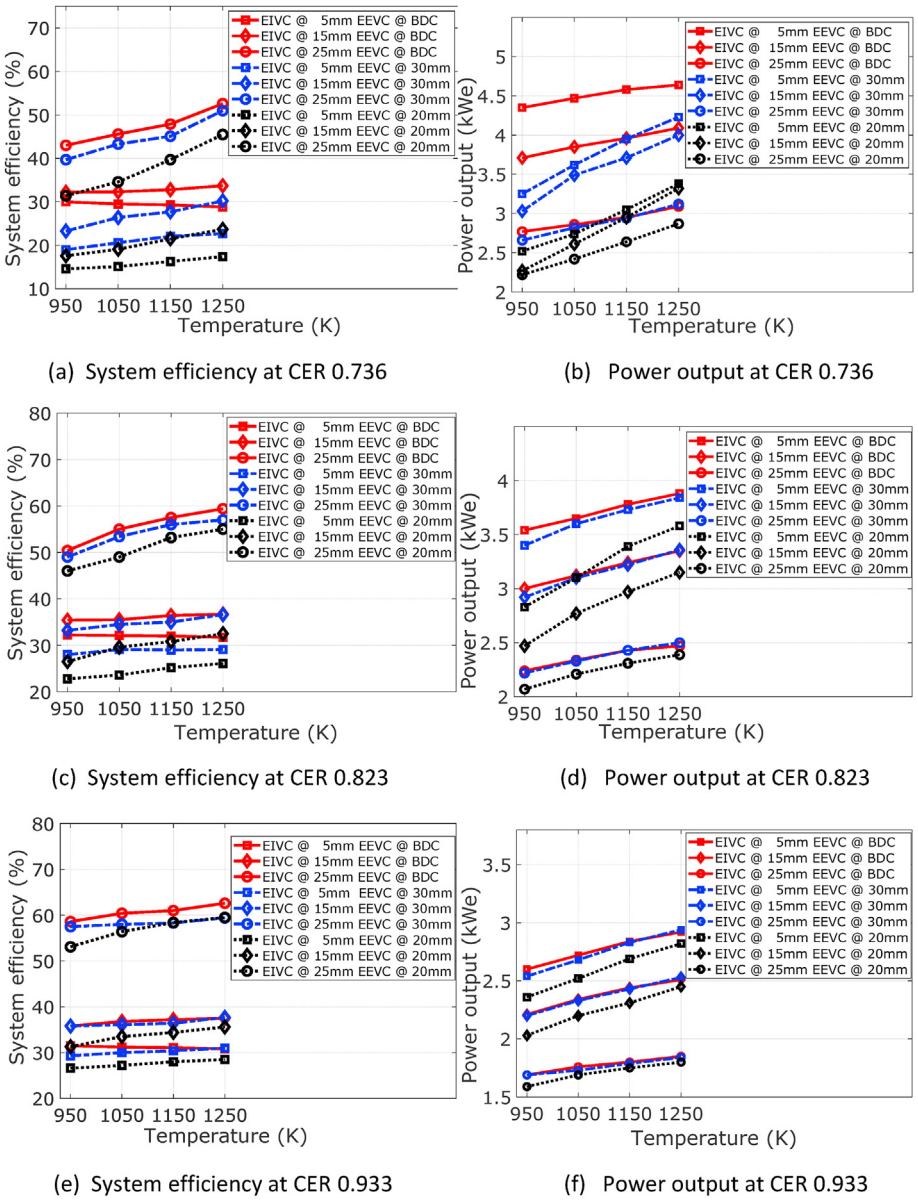

Fig. 9. Temperature effect on system efficiency and power output at different engine conditions.

expander inlet valve-timing window of the LJEG. Beyond this geometric and expander inlet valve timing range, the LJEG system efficiency deteriorated abruptly, or the operational stability was highly undermined, or both the former and latter occur. Notwithstanding, the severity of operating the LJEG beyond these ranges depended on other operational parameters like exhaust valve timing and electric load.

3.3.1. Expander and compressor diameter ratio and valve timing - influence of EIVC

The expander valve timing is one of the important operational parameters that influenced the performance indicators in an LJEG, and the impact of expander inlet timing is shown in Fig. 4. Lower values of system efficiencies were observed at a longer intake duration (e.g. EIVC at 0 mm and 5 mm before the mid stroke), and power output generally increased with extended expander intake duration. It is evident from Fig. 4 that the system efficiency increased with a shorter intake duration. Part of the reason for this was that the end pressure of the expansion process was still relatively high if a prolonged intake valve duration was applied, which indicated that the geometry constraint of the cylinder would not allow the expansion process to be fully conducted if the intake gas mass was too high. Fig. 5 demonstrates that with a longer intake duration (e.g. EIVC 5 mm before the mid stroke), the working fluid energy utilisation level at the end of expansion was relatively lower compared to that of shorter intake durations (e.g. EIVC 15 mm and 25 mm before the mid stroke). Furthermore, with an extended intake duration, a longer piston stroke was achieved (Fig. 6) and energy dissipated through friction was higher, and this friction loss contributed to declining system efficiency at extended EIVC.

EIVC at 25 mm before the mid stroke was the minimum valve opening duration that an LJEG could operate stably with the input parameters stated in Table 1. It also corresponded to the optimal system efficiency of an LJEG regardless of CER or expander exhaust duration adopted. The ability of the LJEG to recover from any disturbance was considerably lower at short intake duration and

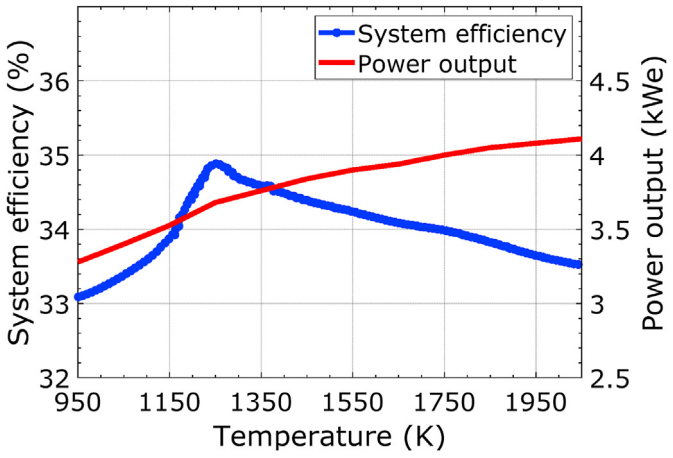

Fig. 10. Power output and system efficiency with expander intake temperature, CER 0.823, EIVC at 10 mm and EEVC at BDC.

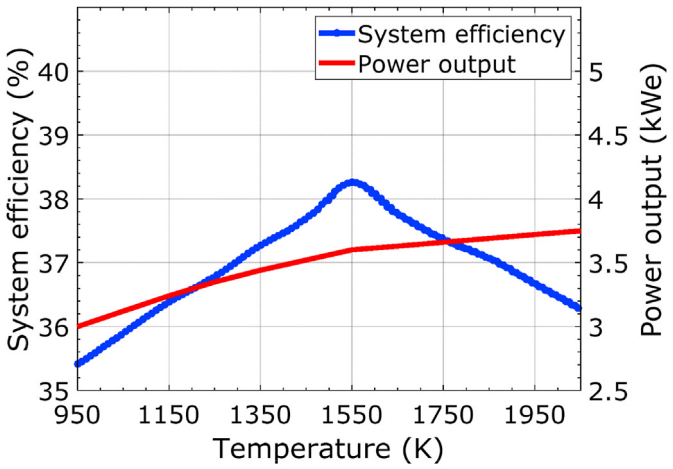

Fig. 11. Power output and system efficiency with expander intake temperature, CER 0.823, EIVC at 15 mm and EEVC at BDC.

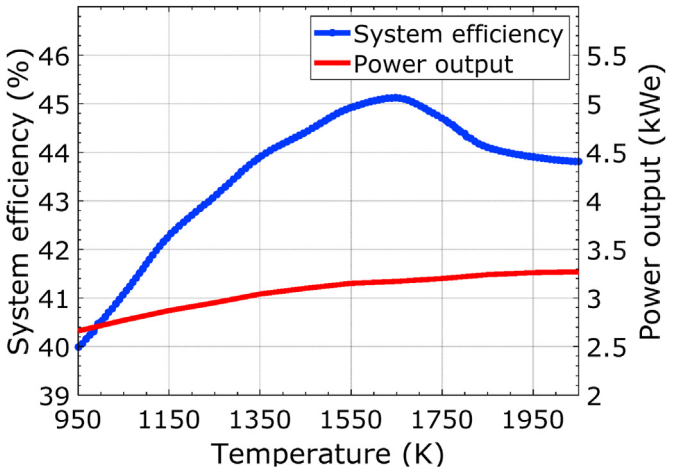

Fig. 12. Power output and system efficiency with expander intake temperature, CER 0.823, EIVC at 20 mm and EEVC at BDC.

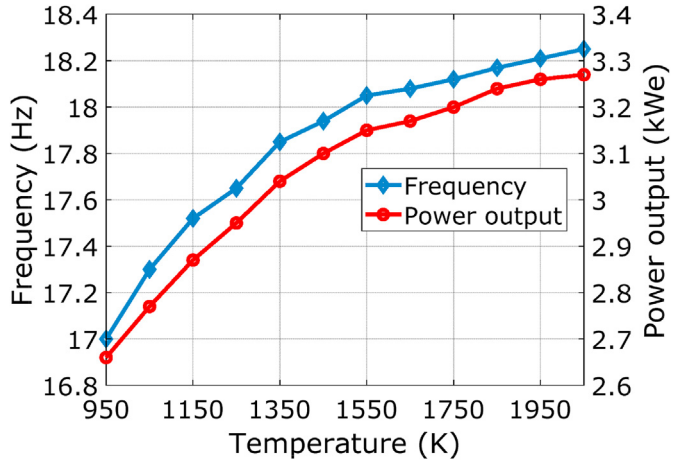

Fig. 13. Power output and system frequency with expander intake temperature, CER 0.823, EIVC at 20 mm and EEVC at BDC.

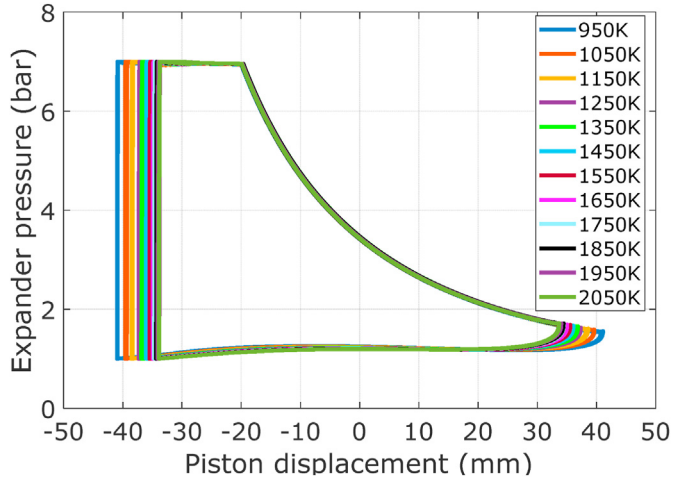

Fig. 14. Expander in-cylinder pressure with displacement, EIVC at 20 mm, EEVC at BDC, CER 0.823 and different intake temperature.

was more robust at extended or longer intake duration.

At the CER of 0.736 or less, the expander intake duration could not extend beyond 5 mm before the mid stroke. This was because the compressor capacity at CER of 0.736 or less could not supply the quantity of fluid needed to sustain the expander intake duration beyond 5 mm before the mid stroke. Therefore, the limit of expander intake duration was dependent on the CER choice of the LJEG.

3.3.2. Expander and compressor diameter ratio and valve timing - influence of EEVC

There was an overall power output and system efficiency improvement made by extending the exhaust valve timing from 20 mm post-mid-stroke to BDC (as evident in Fig. 4a–c). Earlier closure of the expander exhaust valve (expander recompression) led to a decline in the LJEG performance. This drop on performance was because part of the working fluid energy in the active expander is used to compress the trapped exhaust gas in the opposite expander clearance after expansion process, which is clearly demonstrated in Fig. 7. Consequently, adapting the expander exhaust to close at BDC supported both higher system efficiency and power output compared to the cases when the expander

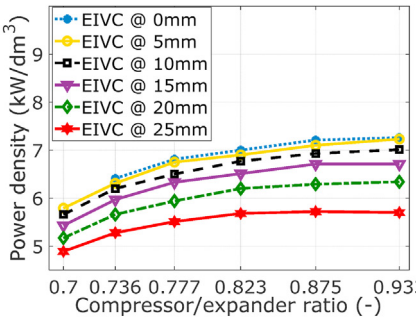

(a) Power density at different engine conditions when the EEVC at BDC

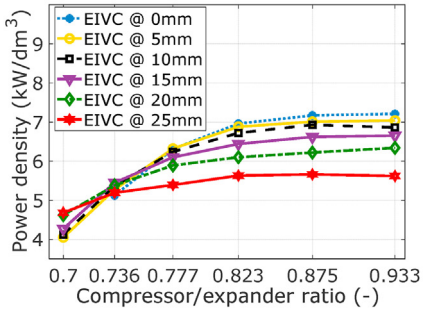

(b) Power density at different engine conditions when the EEVC at 30mm

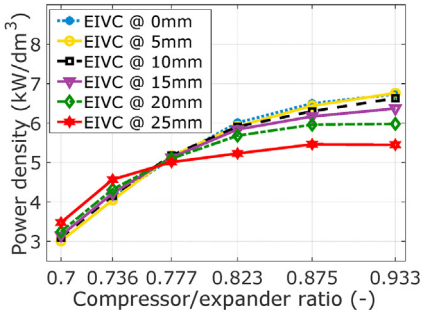

(c) Power density at different engine conditions when the EEVC at 20mm

Fig. 15. Power density at different engine conditions.

exhaust valve closed before BDC. However, due to the nature of a free piston mechanism, BDC is variable while stroke changes. There is an optimal point of BDC for a certain design. Beyond the optimal point with a further increase of stroke, the thermal efficiency and the power output will decrease due to a smaller final clearance volume, therefore huge pressure different during intake stage in the next cycle, as mentioned in Ref. [11]. In this study, strokes under investigation have yet to reach the optimal point. A clear trendy shows that the later the EEVC before BDC, the better was the LJEG performance. In practice, a trade-off between better system performance and control ability of a late EEVC would be necessary. Earlier EEVC might improve the controllability of the LJEG and to implement later EEVC control might pose some challenges.

3.3.3. Expander and compressor diameter ratio and valve timing - influence of CER

The influence of the CER (geometric variable) on the performance indicators of LJEG is presented in Fig. 4. System efficiency improved with an increase in the CER; this was partly because the end pressure of the expansion process was relatively lower with elevated CER compared with the end pressure of the expansion process at lower CER. Similarly, less energy was spent on piston friction due to decreased expander piston perimeter with elevated CER values. Additionally, piston strokes were shorter with increased CER (see Fig. 6); typically, less energy was lost through friction per cycle for shorter piston stroke.

The relationship between the power output and the CER depended on the expander exhaust timing adopted (EEVC). When the expander exhaust valve closed at BDC, as seen in Fig. 4c, the power output and the CER had a linear relationship with a negative gradient for all expander intake timing. If the expander exhaust valve closed at 20 mm after mid-stroke as presented in Fig. 4a, the relationship between the power output and CER was a curve with varying maxima, and the maxima existed between 0.736 and 0.823 CER. However, the location of the maxima was dependent on the expander intake duration. The location of the curve maxima on the independent axis tended to shift from 0.736 towards 0.823 CER with increased expander intake duration. The power output relationship with the CER in Fig. 4b was the combination of the two scenarios presented in Fig. 4a and c. It suggested that if the expander exhaust valve closed before BDC, the power output trend was dependent on both the expander intake and exhaust timing adopted. Therefore, the location of peak power is dependent on the expander exhaust timing adopted. When the exhaust valve closes at BDC, the peak power was located at the least CER. The more advanced the expander exhaust valve closed before the BDC; the peak power location moved towards elevated CER. This implies that recompression in the expander adversely affected the power output further towards low CER. The adverse impact of recompression is proportional to recompression duration, and as well as the expander intake duration; these could be seen in Fig. 4a and b. That is the reason, the location of the peak power moved towards elevated CER with extended intake duration.

3.4. Generator load

The system performance of an LJEG was dependent on the generator load constant, and the load constant was recommended to be limited to an acceptable range to avoid unstable operation. Within this range, it was suggested that the load constant of the generator could be maximised to improve electricity generation efficiency [3]. A generator load constant sweeping was conducted to achieve optimal system efficiency while other parameters remain unchanged. The maximum design value for the generator load constant was 207.3 $N/m \cdot s^{-1}$, and the values of load constant of the generator simulated were the coefficients of the maximum design value, see Equation (22).

$$G = kG_{max} \tag{22}$$

where k represents the generator load coefficient (GLC) and $1 \geq k > 0$, G_{max} represents the maximum design value of the generator load constant.

The GLC at the optimal system efficiency and the corresponding power output at various intake and exhaust valve timings and different CERs are presented in Fig. 8. The results showed that there is an optimal value of generator load constant for every valid combination of the input parameters for optimum system performance. There was a complicated relationship between GLC and power output at different expander intake and exhaust duration, and CER. This complication is caused by different level of impact of recompression on power output due to varying CER and intake duration. At low CER (0.70–0.73) and EEVC before the BDC (Fig. 8a and b), GLC decreased slightly with a longer intake duration, while power output increased simultaneously. At CER of 0.77 and EEVC before the BDC (Fig. 8c), the GLC appeared to be constant across different intake duration while the power output increased with a

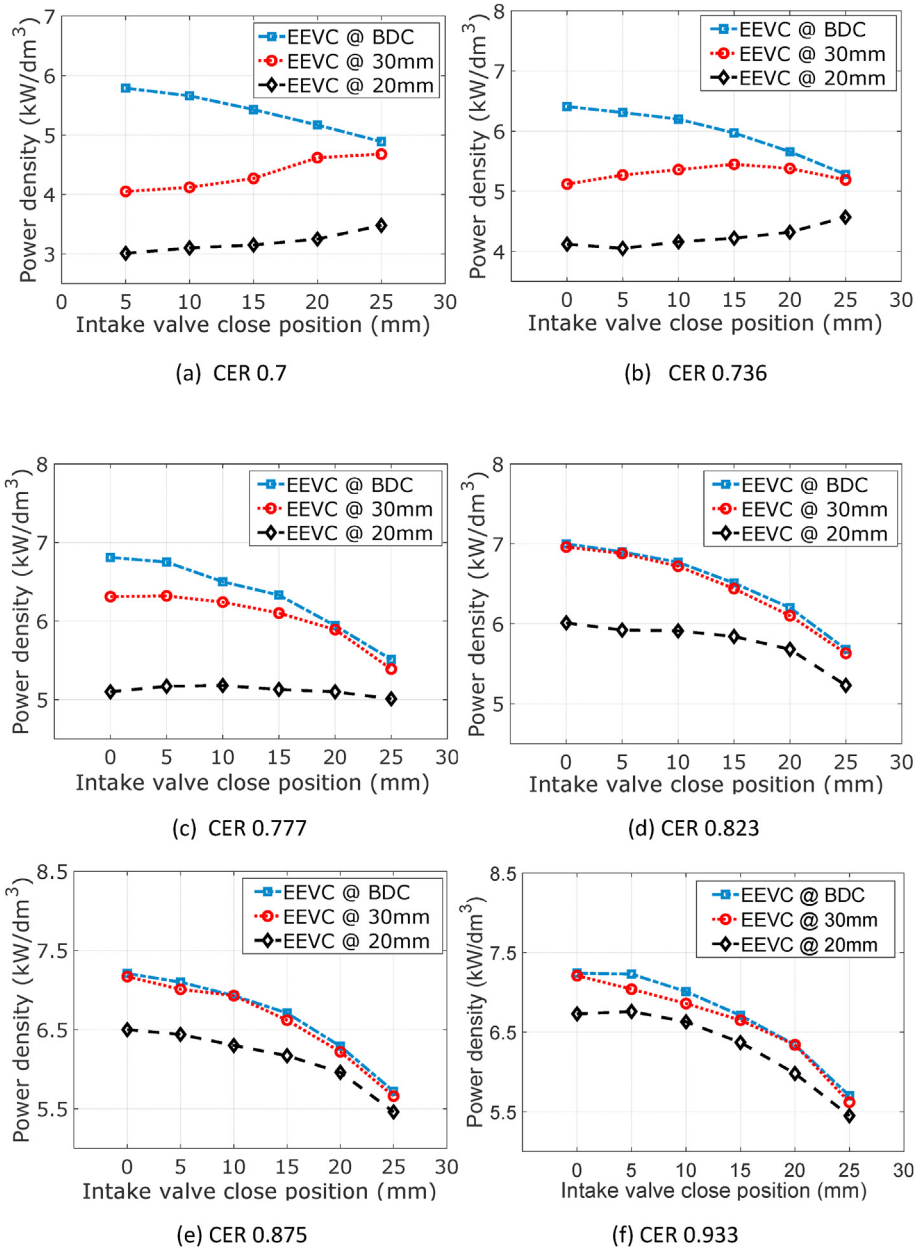

Fig. 16. Power density with different expander intake and exhaust valve timings.

longer intake duration. With high CER above 0.823 and EEVC before the BDC (Fig. 8d–f), GLC increased linearly with extended intake duration while power output also increased with extended intake duration. Generator load coefficient and power output increased with longer intake duration irrespective of CER, provided the exhaust valve close at BDC.

The results in Fig. 8 indicate that if an EEVC at BDC valve timing was adopted, the GLC appeared to stay high at lower CER, and GLC was found to decrease with increased CER. Conversely, it was evident in Fig. 8 that if the EEVC before BDC valve timing was adopted, the GLC was found to be low at lower CER but increased with rising CER. Perhaps an insight into the load influence on different operating conditions is imperative for optimal performance evaluation of the LJEG. Therefore, generator load coefficient searching for various combination of geometric and operational parameters would provide an estimation of the capacity and power density of LJEG with a certain configuration and operational strategy. This, in turn, would guide the design of linear alternator.

3.5. Temperature

The influence of expander intake temperature on system performance was investigated, and the results obtained are presented in Fig. 9. The expander intake temperature was between 950 K and 1250 K (considering any metallurgical constraints), while the other input parameters remained the same as in Table 1. Most of the results obtained show that system efficiency observed the same trend of increasing intake temperature, regardless of CER, provided that the same valve timings were adopted. There was an overall improvement in system efficiency and power output with increased expander intake temperature. An exception to system efficiency improvement with increased temperature occurred

when the EEVC at BDC and the intake duration extended to 5 mm before the mid-stroke (see Fig. 9a, c and 9e). This was due to the operating parameter combination, the optimal system temperature at that combination was around 950 K, and the system efficiency would reduce beyond 950 K; this is because fuel consumption increased with temperature, and with increased temperature, the heat loss to the environment increased. The system power output is proportional to the operating frequency [3] and temperature (see Fig. 13). At this operating parameter combination, the proportionality of frequency increase with temperature is not commensurate with the increase in fuel consumption due to higher temperatures.

The relationship between expander intake temperature and system efficiency and power output was investigated (presuming no metallurgical issue on the LJEG component material selection). The results are presented in Figs. 10–12. System efficiency increased with expander intake temperature until a certain optimal temperature was reached, depending on the adopted valve timings. Above that temperature, system efficiency started to decrease with a further increase in intake temperature. The decrease in efficiency at an increased temperature beyond the optimal temperature is because of the fixed system operating variables, for instance, without the lab facility restriction of the highest compressed air pressure available to drive the poppet valves' pneumatic actuators, the system efficiency would increase with higher intake temperature along with higher pressure ratio beyond 7. At post-optimal temperature, the proportionality of frequency increase with temperature is not comparable with the increased fuel consumption due to higher temperatures. If the other operating variables were not fixed and duly optimised, the system efficiency would increase with intake temperature. Power output increased continuously with intake temperature despite the optimal intake temperature point. However, the changing rate of power output differed in the pre-optimal and the post-optimal performance. In Fig. 11, the changing rate of the power output is one Watt per Kelvin (1 W/K) until it gets to 1550 K (pre-optimal performance). Above 1550 K (post-optimal performance), the changing rate of power output drops to 0.3 Watts per Kelvin (0.3 W/K). It is apparent from Figs. 10–12 that the optimal performance temperature was dependent on the adopted intake valve timing. At shorter intake duration, the frequency per fuel consumption is higher compared with extended intake duration, which results in a higher power density, thus a higher system efficiency. The proportionality of frequency increase with temperature is more subsistent with increased fuel consumption due to higher temperatures at shorter intake duration than extended intake duration. That is why the optimal temperature region shifts to the right at shorter intake duration and this is seen in Figs. 11 and 12 when the EIVC at 15 mm and 20 mm respectively and the optimal intake temperature was around 1550 K and 1650 K respectively.

The relationship between power output and system frequency at varying intake temperature, as depicted in Fig. 13 shows that the power output and the frequency increased with the intake temperature. The expander in-cylinder pressure and the piston stroke in complete cycles are shown in Fig. 14 in terms of varying intake temperature. It could be observed that intake duration became shorter with increased expander intake temperature because lesser working fluid is demanded from the compressor at increased expander intake temperature.

3.6. Power density

The power density (power per expander swept volume) correlation with the CER and valve timings is presented in Figs. 15 and 16. The input parameters were the same as those presented in Table 1. At fixed CER, power density generally increased with extended inlet duration, especially when the EEVC at BDC or very close to the BDC. Additionally, it was evident from Figs. 15 and 16 that the early closure of exhaust valve undermined power density irrespective of the inlet duration adopted. Therefore, at fixed CER, power density was dependent on both expander intake and exhaust duration.

At fixed operational parameters (expander intake and exhaust duration), the power density increased with CER, and this was most likely associated with a reduction in piston stroke at increased CER. Further investigation into Figs. 15 and 16 established that power density increased with CER irrespective of expander intake or the exhaust valve timing adopted. In summary, power density increased with CER and with extended intake and exhaust duration. However, its relationship with intake duration seemed to be interdependent on CER.

4. Conclusions

A new conceptual design of a novel semi-closed-loop Linear Joule Engine Generator (LJEG) with a hydrogen-oxygen-argon reactor is firstly presented, which has the potential to be an alternative chemical-to-electrical energy convertor using zero carbon fuels and emitting zero emissions. A comparison with the open-loop air-standard LJEG and its lab-scale prototype has been conducted to provide validation for further parametric analysis of the proposed LJEG under different operation conditions. In summary, the paper found that:

1) Replacing air with argon as the working fluid would lead to zero emissions, increased system frequency, a minor decrease in indicated power, and over 60% improvement in indicated efficiency. The performance improvement and emission abatement are attributed to the thermo-physical properties of argon.
2) A peak system efficiency of around 40% and 60% was achieved when the compressor/expander diameter ratio is 0.70 and 0.93 respectively, and the exhaust valve closed at the piston bottom dead centre, while the intake closed at 25 mm from mid-stroke.
3) The limit of extension of expander intake duration was dependent on the compressor/expander diameter ratio. Increased compressor/expander diameter ratio supported longer intake duration up to the mid-stroke, and there was a narrow range of expander intake duration possibilities for stable operation in LJEG. The ability of an LJEG to recover from disturbance was considerably lower at shorter intake duration and more robust at longer intake duration.
4) The system efficiency increased with the compressor/expander diameter ratio and decreased with expander extended intake duration. The system efficiency could be improved by extending the expander exhaust duration, and optimal efficiency was achieved if the expander exhaust duration was extended to the piston bottom dead centre.
5) Power output generally increased with longer expander intake duration, and the relationship between power output and the compressor/expander diameter ratio was dependent on the expander exhaust duration adopted. Power output was improved by extending the expander exhaust duration. At any set of parameters, peak power was achieved if the expander exhaust duration was extended to the piston bottom dead centre. A peak power output of over 4.7 kW was achieved at expander intake temperature of 1073 K, low compressor/expander diameter ratio (0.7–0.73) and when the expander inlet valve closes between 5 mm and 0 mm from the mid-stroke.
6) Piston stroke decreased with increased compressor/expander diameter ratio, and power density increased with both compressor/expander diameter ratio and extended inlet and exhaust duration.

7) For every set of operating conditions, there was a particular range of electric load that could ensure optimum system performance. Therefore, the system efficiency could be improved with a satisfactory electric load match for different operating conditions.
8) The system operating temperature for optimal performance was dependent on the adopted intake valve timing. However, a clear trend emerged that longer intake duration leads to lower optimal temperature while shorter intake duration leads to a higher optimal temperature.

Author contribution

Ugochukwu Ngwaka: Conceptualisation, Software, Investigation, Writing – original draft, Dawei Wu: Methodology, Validation, Writing – review & editing, Supervision, Julian Happian-Smith: Writing – review & editing, Supervision, Boru Jia: Software, Writing – review & editing, Andrew Smallbone: Data curation, Writing – review & editing, Supervision, Chidiebere Diyoke: Formal analysis, Writing – review & editing, Anthony Paul Roskilly: Resources, Supervision

Declaration of competing interest

The authors declare that they have no known competing financial interests or personal relationships that could have appeared to influence the work reported in this paper.

Acknowledgement

This work was funded by the UK EPSRC (Engineering and Physical Sciences Research Council) through the project: A Zero-Emission Closed-loop linear-Joule CYcle (ZECCY) engine generator (EP/R041970/1, EP/R041970/2).

References

[1] Mikalsen R, Roskilly AP. The free-piston reciprocating Joule cycle engine: a new approach to efficient domestic CHP generation. in *International Conference on Applied Energy* 2012;2012.
[2] Wu D, Roskilly AP. Design and parametric analysis of Linear Joule-cycle Engine with out-of-cylinder combustion. in *Energy Procedia* 2014. https://doi.org/10.1016/j.egypro.2014.11.1034.
[3] Jia B, Wu D, Smallbone A, Ngwaka UC, Roskilly AP. Dynamic and thermodynamic characteristics of a linear Joule engine generator with different operating conditions. Energy Convers Manag 2018;173. https://doi.org/10.1016/j.enconman.2018.07.098.
[4] Bell MA, Partridge T. Thermodynamic design of a reciprocating Joule cycle engine. Proc Inst Mech Eng Part A J Power Energy 2003. https://doi.org/10.1243/095765003322066475.
[5] Creyx M, Delacourt E, Morin C, Desmet B, Peultier P. Energetic optimization of the performances of a hot air engine for micro-CHP systems working with a Joule or an Ericsson cycle. Energy 2013. https://doi.org/10.1016/j.energy.2012.10.061.
[6] Moss RW, Roskilly AP, Nanda SK. Reciprocating Joule-cycle engine for domestic CHP systems. Appl Energy 2005. https://doi.org/10.1016/j.apenergy.2004.03.007.
[7] Lontsi F, Hamandjoda O, Fozao K, Stouffs P, Nganhou J. Dynamic simulation of a small modified Joule cycle reciprocating Ericsson engine for micro-cogeneration systems. Energy 2013. https://doi.org/10.1016/j.energy.2013.10.061.
[8] Touré A, Stouffs P. Modeling of the ericsson engine. Energy 2014;76:445–52. https://doi.org/10.1016/j.energy.2014.08.030.
[9] Wu D, Jalal AS, Baker N. A coupled model of the linear Joule engine with embedded tubular permanent magnet linear alternator. in *Energy Procedia* 2017. https://doi.org/10.1016/j.egypro.2017.03.571.
[10] Jia B, Wu D, Smallbone A, Lawrence C, Roskilly AP. Design, modelling and validation of a linear Joule Engine generator designed for renewable energy sources. Energy Convers Manag Jun. 2018;165:25–34. https://doi.org/10.1016/J.ENCONMAN.2018.03.050.
[11] Ngangué MN, Stouffs P. Dynamic simulation of an original Joule cycle liquid pistons hot air Ericsson engine. Energy 2020;190. https://doi.org/10.1016/j.energy.2019.116293.
[12] Creyx M, Delacourt E, Morin C, Desmet B. Dynamic modelling of the expansion cylinder of an open Joule cycle Ericsson engine: a bond graph approach. Energy May 2016;102:31–43. https://doi.org/10.1016/J.ENERGY.2016.01.106.
[13] Ngwaka U, et al. Evaluation of performance characteristics of a novel hydrogen-fuelled free-piston engine generator. Int J Hydrogen Energy 2020. https://doi.org/10.1016/j.ijhydene.2020.02.072.
[14] Ngwaka UC, Diyoke C, Anosike N. Single zone, zero dimensional model of diesel multiple-injection. Energy Power Eng 2016:297–312. https://doi.org/10.4236/epe.2016.89028. 08, no. 09.
[15] Shahsavan M, Morovatiyan M, Mack JH. A numerical investigation of hydrogen injection into noble gas working fluids. Int J Hydrogen Energy 2018;43(29):13575–82. https://doi.org/10.1016/j.ijhydene.2018.05.040.
[16] Shahsavan M, Morovatiyan M, Mack JH. A computational investigation of nonpremixed combustion of natural gas injected into mixture of argon and oxygen. J Eng Gas Turbines Power Aug. 2019;141(8). https://doi.org/10.1115/1.4043277.
[17] R. V. Ravikrishna and A. B. Sahu, "Advances in understanding combustion phenomena using non-premixed and partially premixed counterflow flames: a review," Int J Spray Combust Dyn, vol. 10, no. 1. SAGE Publications Inc., pp. 38–71, 01-Mar-2018, doi: 10.1177/1756827717738168.
[18] Hafiz NM, Mansor MRA, Wan Mahmood WMF. Simulation of the combustion process for a CI hydrogen engine in an argon-oxygen atmosphere. Int J Hydrogen Energy Jun. 2018;43(24):11286–97. https://doi.org/10.1016/J.IJHYDENE.2018.05.022.
[19] Kuroki R, Kato A, Kamiyama E, Sawada D. Study of high efficiency zero-emission argon circulated hydrogen engine. In: SAE technical paper series; 2010. https://doi.org/10.4271/2010-01-0581.
[20] Mansor MRA, Nakao S, Nakagami K, Shioji M, Kato A. Ignition characteristics of hydrogen jets in an argon-oxygen atmosphere. in *SAE Technical Paper Series* 2012. https://doi.org/10.4271/2012-01-1312.
[21] Deng J, Zhong H, Gong Y, Gong X, Li L. Studies on injection and mixing characteristics of high pressure hydrogen and oxygen jet in argon atmosphere. Fuel Aug. 2018;226:454–61. https://doi.org/10.1016/j.fuel.2018.04.038.
[22] Zhang E, et al. Cyclic variations of argon power cycle engine with fuel of hydrogen. In: SAE technical paper series; 2017. https://doi.org/10.4271/2017-01-2409.
[23] Gong Y, Zhan Y, Deng J, Wu Z. Experimental and numerical study on combustion characteristics of hydrogen-argon jet in a hot vitiated Co-flow. SAE Tech. Pap. 2018.
[24] Killingsworth NJ, Rapp VH, Flowers DL, Aceves SM, Chen JY, Dibble R. Increased efficiency in SI engine with air replaced by oxygen in argon mixture. Proc Combust Inst 2011. https://doi.org/10.1016/j.proci.2010.07.035.
[25] Aznar MS, et al. Experimental investigation of port and direct injection strategies for internal combustion engines with argon as the working fluid. in *Proceedings of the European Combustion Meeting* 2017;2017. https://doi.org/10.17605/OSF.IO/PT67Q.
[26] Aznar MS, Chorou F, Chen J-Y, Dreizler A, Dibble RW. Experimental and numerical investigation of the argon power cycle. In: ASME 2018 internal combustion engine division fall technical conference; 2018.
[27] Mansor MRA, Shioji M. Investigation of the combustion process of hydrogen jets under argon-circulated hydrogen-engine conditions. Combust Flame 2016. https://doi.org/10.1016/j.combustflame.2016.07.032.
[28] Mansor MRA, Shioji M. Characterization of hydrogen jet development in an argon atmosphere. In: Yao T, editor. Zero-carbon energy Kyoto 2012. Green energy technol. Tokyo: Springer; 2013. p. 133–40.
[29] Drell IL, Belles FE. Survey of hydrogen combustion properties. 1957.
[30] Ngwaka U, Jia B, Lawrence C, Wu D, Smallbone A, Roskilly AP. The characteristics of a Linear Joule Engine Generator operating on a dry friction principle. Appl Energy 2019;237. https://doi.org/10.1016/j.apenergy.2018.12.081.
[31] Polinder H, Slootweg JG, Hoeijmakers MJ, Compter JC. Modelling of a linear PM machine including magnetic saturation and end effects: maximum force to current ratio. In: Iemdc 2003 - IEEE international electric machines and drives conference; 2003. https://doi.org/10.1109/IEMDC.2003.1210328.
[32] Feng H, Guo C, Jia B, Zuo Z, Guo Y, Roskilly T. Research on the intermediate process of a free-piston linear generator from cold start-up to stable operation: numerical model and experimental results. Energy Convers Manag Aug. 2016;122:153–64. https://doi.org/10.1016/J.ENCONMAN.2016.05.068.
[33] Chase Jr MW. NIST-JANAF thermochemical tables fourth edition. J. Phys. Chem. Ref. Data, Monogr. 1998;9.